Different Tracers Give Different Gravitational Mass Distributions

Dalia Chakrabarty[1]

Department of Statistics University of Warwick, Coventry CV4 7AL, U.K. e-mail: d.chakrabarty@warwick.ac.uk

December 17, 2009

ABSTRACT

Context. Charting the extent and amount of dark matter (DM) in the Universe is highly appealing but is equally hard since it is only through the interpretation of its effect that we can track the DM distribution, i.e. the problem is fundamentally inverse. Given the implementational problems, it is non-trivial to quantify the effects of DM on the motion of individual test particles in an elliptical galaxy, with the aim of identifying its total gravitational (i.e. luminous+dark) mass distribution; expectedly, this has caused controversy.

Aims. Leaving such technical details aside, in this article we report on the danger of the very notion that test particle velocities can reliably imply total mass distribution in galaxies.

Methods. We expose the fallibility of this mass determination route, by undertaking a non-parametric Bayesian analysis (using the algorithm CHASSIS) of the observed line-of-sight velocities of individual test particles belonging two distinct particle (or mass tracer) populations: planetary nebulae (PNe) and globular clusters (GCs) that span the outskirts of the galaxy NGC 3379.

Results. The PNe and GC data are shown to be drawn from independent phase space density distributions and total gravitational mass density distributions that are derived from implementation of the two kinematic data sets are found to be significantly different, leading to significant (at 1-σ level) differences in the corresponding solutions for the gravitational potential. CHASSIS currently assumes isotropy in phase space, so this assumption is tested with a robust Bayesian hypothesis test; the GC velocities are found to be more supportive of the assumption of isotropy than are the PNe data. We find that this recovered difference in the state of isotropy between the phase space distributions that the data are drawn from, cannot be used to reconcile the differences in the recovered gravitational mass density distributions.

Conclusions. This recovered dichotomy in the potential structure of the galaxy is indicative of the multi-stability of the dynamical system at hand, i.e. the galaxy. In light of this, we advance the risk involved in the interpretation of gravitational mass distributions obtained from individual tracer samples, as equivalent to the mass distribution of the whole galaxy.

Key words. Galaxies: kinematics and dynamics, dark matter; Methods: Bayesian, hypothesis testing

1. Introduction

NGC 3379, or M 105, seems to have initiated its journey within the observational domain, in neglect - though Pierre Mechain is credited with its discovery in 1781, it did not initially make it to Messier's catalogue. Amends were made later in 1947, when it was among four new objects that were "added to the accepted list of Messier's catalogue as nos. 104, 105, 106 and 107" (from Helen Sawyer, 1947). In spite of this early

Send offprint requests to: Dalia Chakrabarty

inattention, NGC 3379 has recently been in vogue. Romanowsky et. al (2003) had advanced the idea that this system is one of the five “naked galaxies”, the mass distributions of which were tracked with the Planetary Nebula Spectrograph (PNS). Such claims were contested by Dekel et. al (2005), though Douglas et. al (2007) defend the earlier result of Romanowsky et. al (2003) by analysing the kinematic data of 214 planetary nebulae (PNe) in NGC 3379.

Dekel et. al (2005) advance the possibility that NGC 3379 might in actuality be a triaxial system and that it is this intrinsic asphericity that causes the measured line-of-sight projected velocity dispersion (σ_p) to appear less than what it is, for certain inclinations. However, Douglas et. al (2007) argue that such a geometric reasoning, though possible, is unlikely to be a plausible explanation for the other three naked galaxies that were reported by Romanowsky et. al (2003). Additionally, the suggestion that it is the idiosyncracy of this system that the detected PNe data might be tracing a sample of younger stars, rather than the stellar population as a whole, was judged implausible by Douglas et. al (2007) based on the rarity of such an occurrence within a single system, with the sole identification of the presence of multiple PN populations in NGC 4697 (Sambhus, Gerhard & Mendez 2006; Sambhus et al. 2005).

However, the most pressing concern of Dekel et. al (2005) is the possibility that radial anisotropy might be introduced as a result of a merger; Douglas et. al (2007) disagree that this could explain the identification of the low dark matter content in NGC 3379, given that the existence of anisotropy was included in the data-fitting process employed in Romanowsky et. al (2003). They stress that the anisotropy profile recovered from the PNS data and that obtained from the simulations presented in Dekel et. al (2005), are similar in nature. de Lorenzi et al. (2009) confirm that the degeneracy between radial anisotropy and mass is the cause for the PNe data to not strongly constrain the gravitational mass distribution of NGC 3379. Weijmans et al. (2009) cannot infer the distribution of the total gravitational mass distribution in this galaxy since the halo contribution is a model parameter.

Similar concerns about the mass-anisotropy degeneracy have repeatedly been voiced by various workers in the field of mass estimation from tracer kinematics (Łokas & Mamon 2003; Koopmans 2006; Côté et al. 2001, 2003). The relevant question to ask would be: is the uncertainty in mass estimates, implied by our lack of information about the prevalence of anisotropy, so large that we cannot conclude anything significant about the mass distribution in the system? If the response is in the affirmative, then of course it is futile to seek a solution for the mass density from tracer kinematics. Recovering the host galaxy mass distribution, while incorporating full-fledged anisotropy, requires the tracer kinematic sample size to exceed typical numbers - in fact, the sample of 214 planetary velocities that is available for NGC 3379, represents one of the relatively larger samples available. If on the other hand, our analysis can - based upon the limited measurements and the assumptions invoked to tackle the lack of anisotropy estimates - allow us to infer usable information about the mass distribution of the system, then it still makes sense to undertake such analysis. Of course, such inferred mass distributions will have to be qualified adequately, in light of the relevant assumptions.

In this contribution, we report on an investigation of the validity of the usage of tracer kinematics in the determination of the mass of the host galaxy. This is done in reference to the elliptical galaxy NGC 3379, which is the only elliptical galaxy yet, for which kinematic information is available for individual members of two tracer samples that pertain to two separate classes (PNe and GCs), over an extensive radial range spanning the outer parts of the galaxy (radius $\gtrsim 5R_E$). The implication of the analysis of these two independent data samples, on the state of stability of the system potential, is what the paper aims to arrive at.

The undertaken analysis is inverse in nature and is performed with the Bayesian algorithm CHASSIS under the assumptions of spherical geometry and the necessary assumption of phase space isotropy (given the small GC data sample); relaxation of the latter assumption is being explored currently (Chakrabarty & Saha, in preparation). CHASSIS has been calibrated against N-body descriptions of star clusters (Chakrabarty

& Portegies Zwart 2005) and has been applied to gauge the total mass density distributions in various systems (Chakrabarty & Saha 2001; Chakrabarty 2006; Chakrabarty & Raychowdhury 2008).

The input data used in the work include LOS velocities of 164 planetaries (PNe) from the PNS survey (Douglas et. al 2007) and of 29 globular clusters (GC) that were reported by (Bergond et. al 2006). Given that an assumption of isotropy is questionable, Bayesian significance testing of the goodness of this assumption will be undertaken for each data input.

2. Context

The basic motivation behind our work is to check the effect of distinct tracer kinematic data sets in determining the gravitational mass distribution of a given galactic system. If the data sets imply different $\sigma_p(r)$ and number density ($\nu(r)$) profiles, we can infer that the data are drawn from distinct phase space distributions, though we tend to expect that analysis of kinematics of tracer samples from a given galaxy will recover concurrent total mass density distributions. This expectation arises out of the tacit assumption that all tracer orbits experience the same potential, which if it were true, would require the galactic potential to possess a unique minima.

A robust comparison of mass distributions obtained from the analysis of two different kinematic data sets, would first need to be examined in light of the support that each data set offers to the assumptions inherent to the used scheme. The aim of such an exercise is to ascertain if the differences between the derived mass profiles can be reconciled by invoking the discord between the assumptions and the data. If such reconciliation is not possible and the data are drawn from two distinct parts of phase space of the same system, then by the process of elimination, we are left to question the other assumption, namely, all tracer populations sit in a unique galactic potential.

The alternative picture corresponds to some orbits of a certain tracer population confined to a potential well that is independent of another potential well in which another tracer sample sits (Thompson & Stewart 2001). While crossing of the potential barriers between neighbouring wells is possible, (discussed in Section 9), in general, it will be true that some orbits will evolve under a local potential and analysis of their kinematics will therefore imply a gravitational mass distribution that is characteristic of this local potential well, as distinguished from the full galactic potential.

The structure of the conventionally used Jeans Equation formalism does not suggest any a-priori physics for anticipating the recovery of a unique enclosed mass distribution from the implementation of independently observed $\sigma_p(r)$ and $\nu(r)$ distributions of distinct tracers. Therefore, the recovered mass distributions will not be concurrent unless a conspiracy exists between the gradients of these independently observed distributions and the anisotropy parameter, at all r. Such fine-tuning is unrealistic, especially in light of the fact that different tracer populations evolve in different ways, over independent time-scales. Thus, if any operational mass determination scheme implies different mass distributions from distinct kinematic data, it is not altogether surprising.

3. Method

The modus operandi that is adopted in this work is delineated below.

1. PNe and GC data are respectively ported into CHASSIS and physically relevant system characteristics are recovered.
2. Support given to the assumption of phase space isotropy, by each data set, is tested, using a new statistical test that is discussed.

3. If the gravitational mass density distributions obtained from runs performed with the two distinct data sets are found to be significantly different, we check if considerations of differential adherence to the assumption of isotropy by the two data sets could bridge this noted difference. In order to ascertain this, we invoke trends in the density solution with changes in the status of isotropy in the data, within the paradigm of CHASSIS.
4. If noted difference in recovered mass density cannot be bridged as above, then the remaining assumption of uni-stable galactic potential is considered to be refuted.

Thus, this aforementioned process of ratiocination is expected to help elucidate the dynamics of this galaxy.

It is to be mentioned that there is yet another assumption that we have ignored till now - we assume the system to be in equilibrium. This is an assumption, which if we assume is invalidated in the data, no analysis such as CHASSIS or Jeans equation can be undertaken. In other words, we cannot test for the validity of this assumption. Therefore, whatever our conclusions are, will be subject to the validity of the system being in equilibrium.

4. CHASSIS

CHASSIS is an inverse Bayesian non-parametric algorithm that uses MCMC optimisation to recover the total gravitational potential $\Phi(\cdot)$ and the phase space density distribution function $f(\cdot)$ of a host system, by analysing a sample of one or more components of the velocity vector of individual tracers that reside in this host (see Equation 7 below and Chakrabarty 2009 for details). Actually, $\Phi(\cdot)$ is calculated at each iterative step from the total mass density $\rho(\cdot)$ using Poisson equation. We assume a *spherical geometry* and *isotropy in phase space space*: $\rho = \rho(r)$ and $f = f(E)$ where r is the spherical radius and E the energy. We are basically looking for $\Pr(f(E), \rho(r)|data)$ and estimate this in a Bayesian way. The r and E spaces are independently discretised and $\rho(r)$ and $f(E)$ are represented by constructions that are each akin to one dimensional bar-graphs or the $\rho - histogram$ and $f - histogram$. As we see, the target measure is defined on a high dimensional functional space, the dimensionality N_d being given by the discrete r and E bins that the relevant ranges of radius and energy are binned into.

However, in this search for the most likely configuration, we do not have any prior notions about $f(E)$ or $\rho(r)$, except that we require:

$$\begin{aligned} &f(E) \geq 0, \quad \text{and} \quad \rho(r) \geq 0, \\ &\frac{df(E)}{dE} < 0 \quad \text{and} \quad \frac{d\rho}{dr} < 0. \end{aligned} \tag{1}$$

Other than such monotonicity & positivity conditions, the sought functions are retained as completely free-form, i.e. we use uniform priors.

The algorithm starts with seeds for the $f(E)$ and $\rho(r)$ and at the beginning of each step, the f and ρ histograms are tweaked slightly over their past form, in scale and shape[1].

The maximal region of the likelihood function is sampled using MCMC - we use Metropolis-Hastings (Hastings 1970; Metropolis et. al 1953; Tierney 1994; Tanner 1996; Gelman et. al 1995). The recovered $f(E)$ and $\rho(r)$ are ascribed ± 1-σ uncertainties corresponding to the ± 1-σ extent of the wandering within the

[1] Given that the data points are conditionally independent and identically distributed, the target measure is in product form. The jump proposal uses a random Gaussian deviate. Recalling that the gravitational mass density is a physical density, at radius r, in step $t + \delta t$ it is $\rho^{t+\delta t}(r) = \rho^{t+\delta t}(r + \delta r) + \Delta^t(r)$ where $\Delta^t(r) = [\rho^t(r) - \rho^t(r + \delta r)]\sqrt{2s}\mathcal{R}$, where $\mathcal{R} \sim \mathcal{N}(\prime, \infty)$ and the dispersion $s \sim N_d^{-\alpha}$, with $\alpha \in [0.25, 0.5]$ typically. The updating for $f(E)$ is similar. The MCMC details are motivated by Gelman, Roberts & Gilks (1996); Roberts, Gelman & Gilks (1997); Roberts and Sahu (1997); Roberts & Rosenthal (2001)

maximal region in the likelihood function. The observed error bars in velocity are convolved in, assuming a Gaussian error distribution for the observed errors.

The quantities that are directly recovered from the algorithm are used to generate other physically interesting distributions, such as the enclosed mass and velocity dispersion profiles.

4.1. Overestimation of mass

Now, as was discussed in Chakrabarty & Portegies Zwart (2005), CHASSIS bears the peculiarity that an erroneous assumption of velocity isotropy, results in the over-estimation of mass. This can be qualitatively understood as the following. Under the assumption of isotropy, elongated orbits characterised by relatively higher velocities near the inner parts of the galaxy will be mistakenly thought to manifest isotropy. The relatively higher velocities (and their components thereof) measured at low radii will then be misconstrued to represent the orbital speed of the particle, i.e. the orbital speed will be over-estimated at low radii. Therefore, the gravitational mass density $\rho(r)$ will then be over-estimated by CHASSIS - more at smaller than at larger r. Here the radial range over which this over-estimation happens depends on orbital shape. *Thus, the effect of under-representing anisotropy is to spuriously enhance $\rho(r)$ in the inner parts of the galaxy though elsewhere the mass density is correctly identified.* Consequently, the mass thought to be enclosed within a given radius, is an overestimation compared to the true enclosed mass (empirically verified in Chakrabarty et. al 2009, in preparation).

This trend in the solution for $\rho(r)$, in wake of a deviation of the data from the assumption of isotropy is really the reaction of the algorithm to an error. How errors propagate and affect the solutions is dependent on the details adopted in the calculations. Thus, it is expected that if in a Jeans equation calculation, enclosed mass is spuriously enhanced or deflated, depending on whether the anisotropy parameter is over or under-estimated, the same trend will not necessarily be noticed in the solutions obtained with an independent and inverse scheme such as CHASSIS.

5. Why work with an isotropy-assuming algorithm?

Here we discuss the motivation behind choosing to work with the assumption of phase space isotropy, i.e. with $f = f(E)$ rather than have a simple anisotropic representation such as a 2-integral f. From experiments with a 2-integral distribution functions that are currently underway, (Chakrabarty & Saha, 2009), it appears that for sample sizes $\lesssim$100 and velocity measurement errors $\sim$20%, the recovered $\rho(r)$ is marked by very large error bars, by which is implied uncertainties high enough to render the recovered $\rho(r)$ meaningless. Given that the aim of the current work is to compare the effect of the PNe and GC data - where the GC sample has less than 30 data points in it - the choice of an anisotropic $f(\cdot)$ is therefore pointless. Rather, *we find it useful to work with the isotropy-assuming CHASSIS and then undertake a robust statistical test of hypothesis to check if our recovered solutions are biased in the available data.*

6. Results

Runs were conducted with different initial seeds for the gravitational mass density and the $f(E)$, to check for robustness of the answers to seed selection.

6.1. Seeds

In order to establish the independence of the recovered results from the initial choice of the seed ρ and seed f, we have performed multiple runs beginning with distinct seed characteristics. The general form of the seed density $\rho_{seed}(r)$ has been chosen to be:

$$\rho_{seed}(r) = \frac{\rho_0}{\left(\frac{r}{r_c}\right)^{\alpha_1}\left(1+\frac{r}{r_c}\right)^{\alpha_2}}, \tag{2}$$

where ρ_0 is the amplitude determining parameter and α_1, α_2 and r_c affect the shape of the seed density profile. Of these, we find CHASSIS totally unaffected by the choice of ρ_0; convergence is achieved with the other parameters lying in moderately extensive ranges. Such ranges are reflected in the different seeds that we work with (see below).

The seed $f_{seed}(E)$ (where E is energy, with $-1 \leq E \leq 0$), is chosen to be either power-law in form (with the power β) or exponential:

$$\begin{aligned} f_{seed}(E) &= \exp^{-E} \text{ or} \\ &= (-E)^{\beta} \end{aligned} \tag{3}$$

Three different runs performed with the PNe are characterised by seeds that are described as follows.

- PNe-RUN I: r_c=30kpc, α_1=2.8, α_2=1, $f_{seed} = \exp^{-E}$.
- PNe-RUN II: r_c=20kpc, α_1=3.8, α_2=2, $f_{seed} = (-E)^3$.
- PNe-RUN III: r_c=10kpc, α_1=1.8, α_2=3, $f_{seed} = (-E)^5$.

Three different runs performed with the GCs are characterised by the following seeds.

- GC-RUN I: r_c=30kpc, α_1=2.8, α_2=1, $f_{seed} = \exp^{-E}$.
- GC-RUN II: r_c=5kpc, α_1=3.6, α_2=2, $f_{seed} = (-E)^5$.
- GC-RUN III: r_c=10kpc, α_1=3.2, α_2=3, $f_{seed} = (-E)^2$.

The gravitational mass density profiles that are recovered from the three PNe and GC runs are shown in the panels of Figure 1. The overlapping of the density distributions recovered from these assorted runs implies that the obtained results are independent of the initial guess for $\rho(r)$ and $f(E)$. The recovered density profiles bear different degrees of uncertainty depending on the data sizes implemented in the particular run and to a smaller extent, on values to which the different knobs inside our MCMC optimiser are set (for example, the details of the jump probability distribution).

Figure 1 also presents the phase space distribution functions, approximated as isotropic, as recovered from two different runs of CHASSIS, each performed with the kinematic data of a distinct type of mass tracer.

6.2. Recovered $\rho(r)$ and $f(E)$; derived distributions

Given the similarity of the recovered density distributions from different runs performed with a given tracer data, results from a sample PNe run (PNe-RUN I) are compared to those from GC-RUN I. This is shown in Figure 2; it includes comparison between the recovered total mass density $\rho(r)$, enclosed mass $M(r)$, total cumulative mass to light ratio in the B-band $\Upsilon_B(< r)$ and the circular velocity defined by $v_c = \sqrt{GM(r)/r}$.

From the recovered $\rho(r)$, $M(r)$ is estimated. $\rho(r)$ recovered from PNe-RUN I drops much quicker than that from GC-RUN I. This is further reflected in the enclosed mass profile $M(r)$, which flattens out in the result from PNe-RUN I by about 7 kpc, while continuing to rise even at 25 kpc, in GC-RUN I.

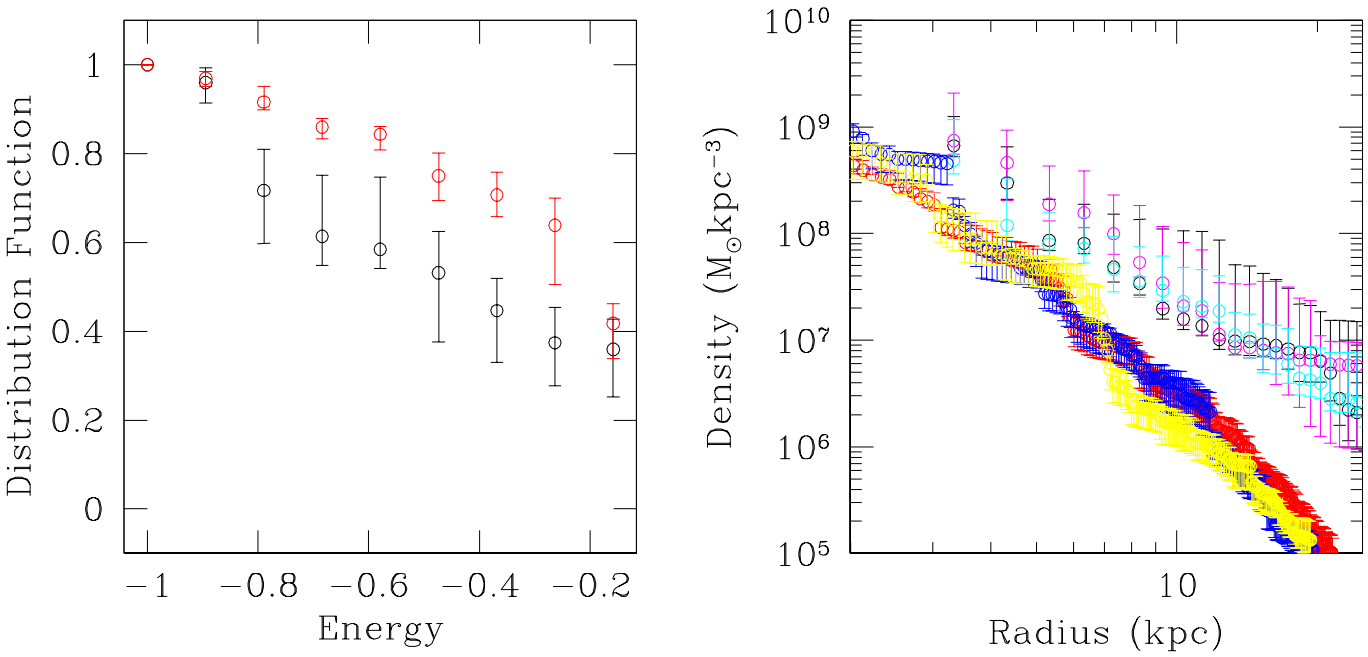

Fig. 1. Right panel: density profiles recovered from the 3 PNe runs and the 3 GC runs. The results of the PNe runs are shown in red, yellow and blue while the density distributions obtained by using the GC kinematics are in black, magenta and cyan. As is apparent from the figure, starting with different seeds results in density profiles that are consistent with each other, as long as the same kinematic tracer sample is used in the analysis. Left panel: isotropic (normalised) phase space distribution functions recovered from PNe-RUN I (in red) and from GC-RUN I (in black). The distribution function is plotted as function of energy.

Now, a flat or constant enclosed mass profile would imply that the quantity defined as akin to the circular velocity ($v_c = \sqrt{GM(r)/r}$), would be falling simply as $r^{-1/2}$, i.e. as in a Keplerian potential. Here G is Newton's Universal Gravitational constant. This quantity is shown in the lower right panel of Figure 2, on which is over-plotted the true Keplerian $r^{-1/2}$ function, normalised by G times the mass that is recovered at r=3R_E, from PNe-RUN I. As is evident from the figure, the true Keplerian fall-off and the v_c estimated from PNe-RUN I overlap very well, though $v_c(r)$ recovered from GC-RUN I is much flatter than the $r^{-1/2}$ fall-off. This is only another way of expressing the fact that $M(r)$ flattens out to a constant mass for PNe-RUN I while it continually rises for GC-RUN I.

6.3. Recovered LOS velocity dispersion

Figure 3 represents the LOS velocity dispersion distributions $\sigma_p(r)$ that are recovered from PNe-RUN I and GC-RUN I. The recovered f is used, in conjunction with the derived ρ, to calculate $\sigma_p(r)$. Again, we notice the significantly flatter shape of the $\sigma_p(r)$ distribution that is obtained from GC-RUN I, as distinct from the steeply falling trend in the distribution estimated from the PNe-RUN I.

It is not surprising that CHASSIS identifies distinct $\sigma_p(r)$ profiles from the implementation of the 2 different kinematic samples. After all, such distinct kinematic data sets would result in the construction of the distinct $\sigma_p(r)$ profiles (which in turn imply distinct phase space density distributions).

6.4. Photometry used for Υ_B estimation

The cumulative Υ profile, in the B-band is shown in Figure 2. The calculation of $\Upsilon(< r)$ of the galaxy requires knowledge of photometry. The surface brightness distribution is the same as used in Douglas et. al (2007) and has been kindly provided by Aaron Romanowsky. It is deprojected in the spherical geometry,

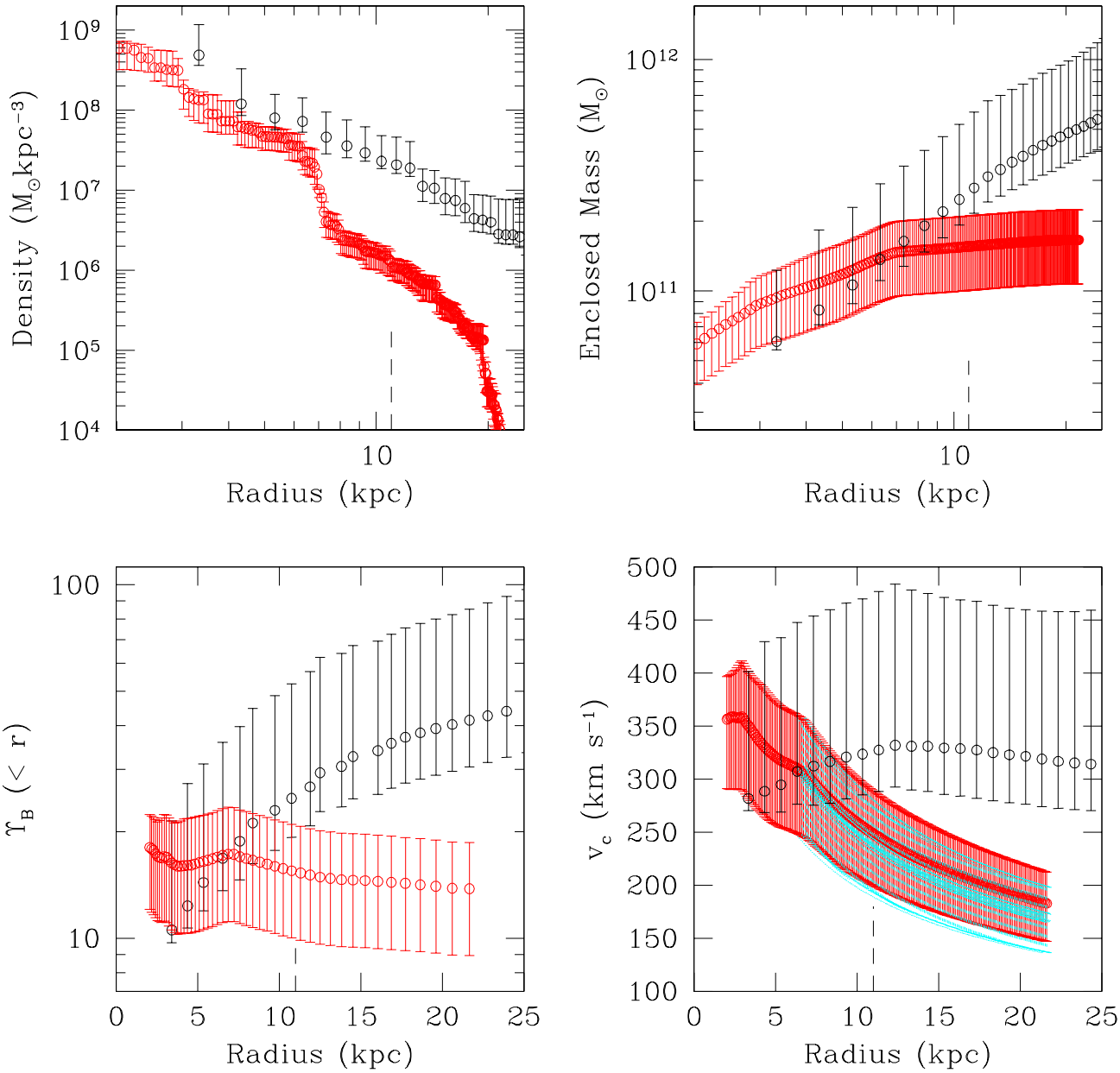

Fig. 2. Top left panel shows the total mass density recovered from PNe-RUN I (in red) and GC-RUN I (in black). The enclosed mass profiles $M(r)$, as extracted from these runs, are represented in the corresponding colours in the top right panel. The lower left panel represents the B-band cumulative mass-to-light profiles $\Upsilon_B(< r)$, estimated from the $M(r)$ recovered from the corresponding run, and the luminosity density shown in Figure 4. The lower right panel shows the radial distribution of the quantity akin to the circular velocity v_c, as obtained from the two runs performed with the two sets of tracers. The points in cyan correspond to the function $r^{-1/2}$, normalised by GM_0, where M_0 is the mass (with errors) found to be enclosed within $3R_E$, from PNe-RUN I.

using the non-parametric deprojection code DOPING (Chakrabarty 2009), to give us the luminosity density distribution $j(r)$ (see Figure 4). Though DOPING can perform deprojection in general triaxial geometries, here we limit ourselves to deprojection under sphericity, since CHASSIS assumes sphericity (and velocity isotropy). In fact, the photometric data used to calculate $j(r)$ in Douglas et. al (2007) were analysed under sphericity too; the deprojection there was performed by fitting analytical distributions to the data. Figure 4 shows the analytical 3-D luminosity density distribution obtained by the fitting method of Douglas et. al

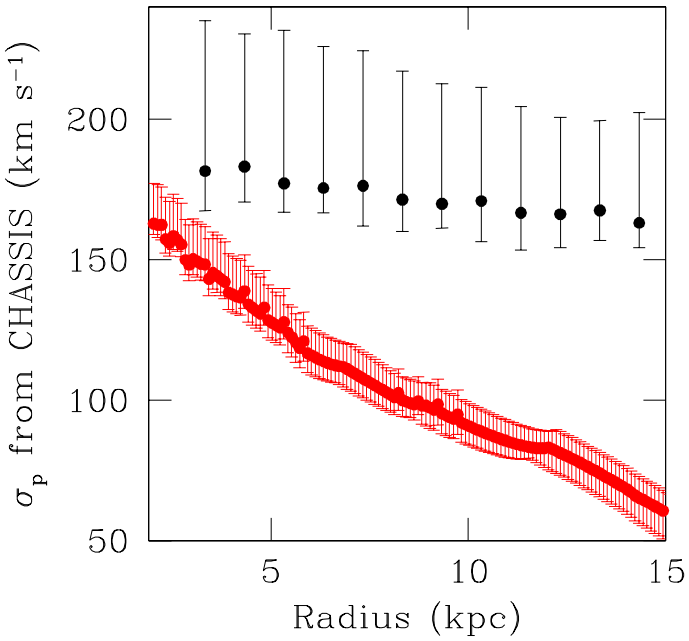

Fig. 3. The LOS velocity dispersion profiles recovered from PNe-RUN I (in red) and from GC-RUN I (in black).

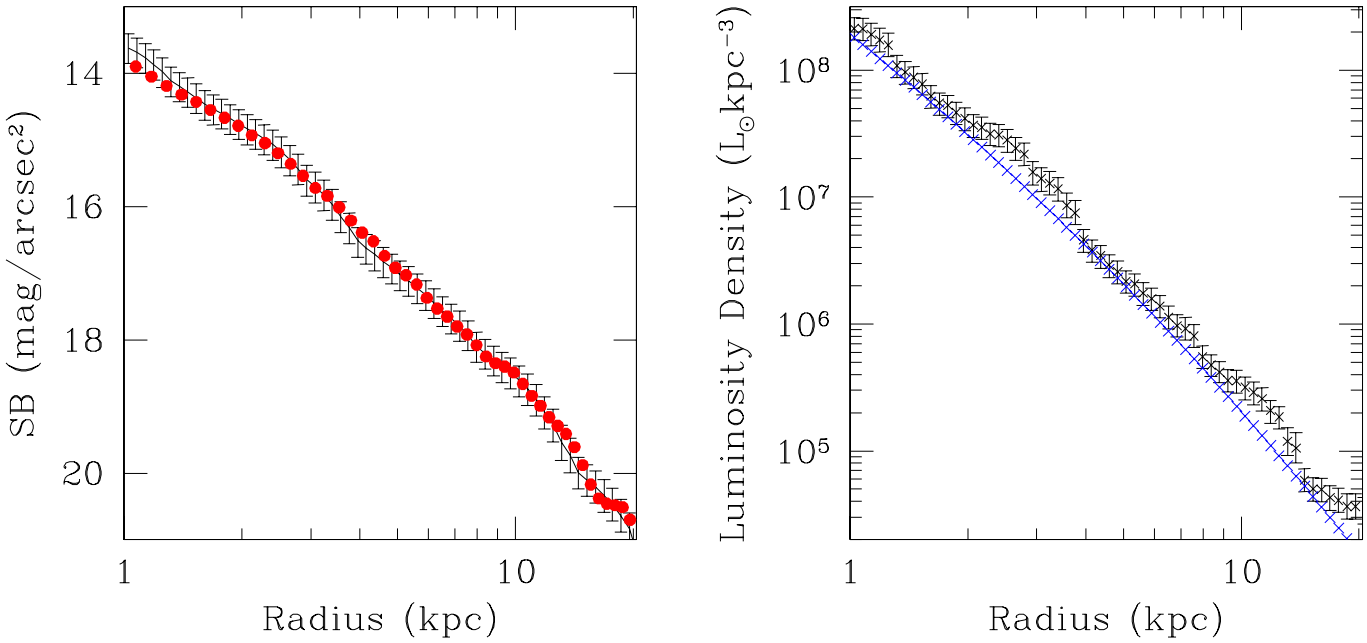

Fig. 4. The points in black in the right panel represent the luminosity density profile ($j(r)$), of NGC 3379, as obtained by deprojecting the surface brightness profile in the *B*-band (shown in red, in the let panel) by the deprojection algorithm DOPING, under an assumption of sphericity. The projection of this deprojected density (in black, in the right panel) is compared to the measured brightness data. The analytical $j(r)$ used by Douglas et. al (2007) is shown in blue in the right panel.

(2007), as compared to the $j(r)$ we recover with DOPING. The luminosity density distributions compare well with each other, though, as expected, the $j(r)$ obtained by Douglas et. al (2007) from fitting is smoother - the undulations in the observed surface brightness is better represented by our recovered $j(r)$.

Our deprojected $j(r)$ is used to calculate the cumulative light distribution, which when compared to $M(r)$, gives us the cumulative mass-to-light ratio $\Upsilon(< r)$. Our results indicate that the mass to light ratios of the outer parts of NGC 3379, as tracked by the PNe velocities is significantly depressed in amplitude compared to that implied by the GC kinematics! Individual consideration of the PNe analysis leads to a "naked" interpretation for NGC 3379, in line with what was suggested by Douglas et. al (2007) and Romanowsky et. al (2003). The

GCs on the other hand, paint a diametrically opposite picture of the galaxy in terms of DM content - in fact, we find the mass-to-light ratios in B to be high enough to suggest that the galaxy is rich in DM, in line with Bergond et. al (2006).

The $\Upsilon(< r)$ recovered from the PNe-RUN, at $5R_E$ lies between 10 and 20. This is slightly higher than what Douglas et. al (2007) advance for NGC 3379, in spite of both mass-to-light calculations having used concurrent luminosity density distributions (see Figure 4). This slight discrepancy is attributed to the assumption of isotropy in our work which artificially augments mass density values wherever anisotropy exists.

This apparently dichotomous view of the potential of a given galaxy is now reviewed via an examination of the validity of the involved assumptions. The principle assumption in CHASSIS is that of phase space isotropy. We now *test* for the support to this assumption offered by the two relevant data samples.

7. Testing for isotropy

Testing of validity of the assumption of isotropy, given the observed data, is an exercise in statistical hypothesis testing. Such test of significance will not *prove* or *disprove* the isotropic nature of phase space of NGC 3379 but will provide a probabilistic estimate of the goodness of the assumption of isotropy in the data. We settle for isotropy and test for the compatibility of our assumption of isotropy with the measured data, using a robust statistical test that has been developed for the purpose at hand.

While traditionally this is typically done by undertaking a calculation of p-values (Kempthorne & Folks 1971), better, more sophisticated techniques also exist, such as the Bayesian evidence measures, a robust example of which is the Fully Bayesian Significance Test or FBST (Pereira & Stern 1999; Pereira, Stern & Wechsler 2008). A highly satisfying aspect of the Bayesian evidence value is that it obeys the Likelihood Principle (Basu 1975; Birnbaum 1962).

p-values provide the probability that the value of the sought measure, given randomly generated data, is at least as inconsistent with the null hypothesis as that corresponding to the observed data is. “Small” p-values imply that the null is unlikely to be true; the definition of “small”ness is traditionally held as 5% significance. Also, the estimation of p-values is an exploration in sample space, while we would prefer to work in parameter space. Most importantly, testing with p-values leads to rejection or non-rejection of the null hypothesis, at the pre-set significance level; the size of the effect cannot be evaluated with p-values. p-values are indeed mired in a web of problems, including the potential to falsely inflate compatibility with the null. A rather severe criticism is presented by Hubbard & Lindsay (2008).

7.1. General FBST - a brief introduction

Given such shortcomings, FBST is a welcome change. Here we discuss the salient features of the general FBST formalism that tests the null hypothesis that the relevant parameter - θ - has a value of θ_0, i.e. $H_0 : \theta = \theta_0$, (say) where θ is assumed to be distributed continuously in the parameter space Θ. Once the essence of FBST is clarified, we move on to *our* implementation of FBST in a non-parametric context; see Chakrabarty (2009) for greater details.

FBST measures the evidence in favour of H_0 by identifying the most likely, H_0-obeying measure (θ^*) and then quantifies the probability of identifying θ that are more likely than θ^*[2]. Such θ comprise the tangential set T. In other words, T is composed of all θ that are more consistent with the observed data ($\{data\}$) than θ^* is.

[2] In other words, FBST requires identification of all θ, the posterior probability corresponding to which is in excess of that of θ^*.

Then the evidence in favour of H_0 is:

$$ev = 1 - \Pr(\theta \in T|\{data\}), \text{ where}$$
$$T = \{\theta : \Pr(\theta|\{data\}) > \Pr(\theta^*|H_0)\}. \quad (4)$$

Here the probability of recovering θ, given the measurements $\{data\}$ is $\Pr(\theta|\{data\})$ and θ^* is the point in Θ space, satisfying H_0, that maximises this probability.

Thus, FBST involves identification of θ^*, followed by integration over T.

7.2. Implementation of FBST

We present below a version of the *ev* calculation, adapted for the case when the measure θ is non-parametrically estimated. This is the first reported implementation of FBST in a non-parametric situation. In this case, the integration of $\Pr(\theta|\{data\})$ over the T is difficult and can be replaced by a case-counting scheme. In our work,

- $\theta \equiv \{\rho - f\}$histogram pairs,
- Θ is the space of all $\{\rho - f\}$histograms,

For us, the null hypothesis is that the data are drawn from an isotropic phase space, i.e.

$$H_0 : \hat{f} = \Psi[E(\sum_i v_i^2/2 + \Phi(r))], \quad (5)$$

where

- $\hat{f}$ is the phase space density from which the *input* kinematic sample is drawn, and
- Ψ is some function: $\Psi > 0$ for $E < 0$ and $\Psi = 0$ otherwise.

We are not sure if the observed GC and PNe data are drawn from isotropic phase space distributions and so test if H_0 is true for each measured sample.

The first step is to identify the $\{rho - f\}$*histogram pair that maximises the posterior, given the null*. This sought ρ^*, f^* pair is the equivalent of θ^* that is defined above. In order to identify this ρ^*, f^* pair, the following construct is used.

Our MCMC optimiser, identifies a range of $\rho(r)$ and $f(E)$ distributions, within a ± 1-σ error band. Using this achieved solution, we generate n samples of N_{data}-sized data sets corresponding to the observables, i.e. v_z, x_p, y_p. Here N_{data} is the size of the observed data and v_z is the LOS velocity coordinate while the coordinates of the particle with LOS velocity v_z, on the 2-D image of the system, are x_p, y_p. Thus, these n generated velocity data sets are drawn from the *isotropic* $f(E)$ recovered by CHASSIS. Let us refer to these generated data sets as $D_{CHASSIS}$. Therefore, kinematic information in $D_{CHASSIS}$ are drawn from a phase space density which is indeed isotropic, unlike the observed data which are not necessarily drawn from an isotropic phase space. In this way, we now have n number of null-obeying data sets $D_{CHASSIS}$.

Next we input each of the n $D_{CHASSIS}$ into CHASSIS, to start n new runs. This generates new sets of $\{\rho - f\}$histograms. In fact, at the end of each step in each of these n new runs, we recover a $\{\rho - f\}$histogram pair - each such pair of functions is obtained under the null[3]. Of all these $\{\rho - f\}$histograms, that which maximises the posterior (the pair ρ^*, f^*) is recognised as our equivalent of θ^*. We record the posterior $\Pr(\rho^*, f^*)$ corresponding to this recovered pair.

Now that the sought ρ^*, f^* pair is spotted, the next step is to find $\{\rho - f\}$ pairs for which the posterior probability exceeds $\Pr(\rho^*, f^*)$. To achieve this, all the histogram solutions that we have recovered from runs of CHASSIS performed with the observed data, are now compared to the recorded $\Pr(\rho^*, f^*)$.

[3] The recovered $\{\rho - f\}$histogram pairs are those that are recorded subsequent to the passage of burn-in.

Let there be a total of N $\{\rho - f\}$histograms recovered from all performed runs of CHASSIS performed with observed data. Out of these, if the number of cases for which $\Pr(\{\rho, f\}|\{data\}) > \Pr(\rho^*, f^*)$, is M, we obtain our *ev* as $1 - M/N$ (Equation 4). Thus, we set:

$$\Pr(\{\rho, f\} \in T|\{data\}) = \frac{M}{N} \tag{6}$$

In line with FBST, the null is rejected for "small" *ev*. This "small"ness can be objectively qualified in terms of minimisation of the loss function (Pereira, Stern & Wechsler 2008; Madruga, Esteves & Wechsler 2001).

7.3. Results from implementation of FBST

The implementation of FBST, as described above, is invoked to estimate if the assumption of isotropy should be rejected, in the two different tracer classes that we deal with.

The estimated *ev* for the different PNe runs are (approximately):

- PNe-RUN I: 0.61,
- PNe-RUN II: 0.58,
- PNe-RUN III: 0.62.

The *ev* values for the three GC runs are:

- GC-RUN I: 0.96,
- GC-RUN II: 0.96,
- GC-RUN III: 0.93.

The results of our quantification of support provided by the data to the assumption of isotropy, are summarised as follows.

- Assumption is more likely to be invalid for the phase space from which the PNe data are drawn than from which the GC data is drawn.
- Isotropy is a good description of the phase space that the GC data in NGC 3379 are drawn from, as in M87 and M49, as reported by Côté et al. (2003) and Côté et al. (2001) respectively.
- The two tracer samples have been drawn from significantly distinct phase space density distributions since the adherence of the two samples to isotropy is significantly different , i.e. *the phase space of NGC 3379 is marked by at least two distinct basins of attractions*.

It merits mention that while an $ev > 0.9$ would support confidence in the assumption of isotropy, the $ev \sim 0.6$ is not small enough to suggest complete rebuttal of the assumption of isotropy by the PNe data. However, all we can objectively infer from our analysis is the comparative adherence of the two data sets, to the assumption of isotropy.

We recall from the previous section that under isotropy, gravitational mass density obtained from GC data is significantly higher than density recovered with PNe data. The question to now ask is *if the higher support to the assumption of isotropy provided by the GC data, over the PNe data, is responsible for this noted difference in the recovered distributions of gravitational mass density*. In order to answer this, we review the trend in the $\rho(r)$ recovered by CHASSIS when isotropy is a mistaken assumption.

8. Can differential adherence to isotropy explain differences?

As was delineated in Chakrabarty & Portegies Zwart (2005), CHASSIS bears the peculiarity that when the data are taken from an anisotropic phase space distribution, $\rho(r)$ recovered under the erroneous assumption

of isotropy, is an overestimation. This trend can be used to infer the corrections that need to be imposed on the recovered mass density distributions, in light of our testing of the status of anisotropy in the true phase space from which the input kinematic samples are each drawn.

As marked in the third point in the itemised list in Section 3, we now check if this differential favouring of the assumption of isotropy can help bridge the difference noticed in $\rho(r)$ recovered by CHASSIS, when the two different data are used.

The PNe data are sampled from a phase space density distribution that is more anisotropic than the GC data. Therefore, the trend in the solution with incorporation of the correct degree of anisotropy into the PNe data analysis implies that the recovered density would no longer be overestimated, i.e. the recovered $\rho(r)$ would then be lower, than that recovered under the assumption of isotropy. However, the incorporation of the true status of anisotropy will not trigger much change in the $\rho(r)$ derived by CHASSIS from the GC data. In other words, incorporating the correct amount of anisotropy into the analyses of the two data samples will result in a widening of the gap between the recovered mass density distributions. Thus, *accounting for anisotropy will enhance the difference between the density profiles obtained from the PNe and GC data sets*.

Thus, we conclude that differential adherence of the two data sets, to phase space isotropy, cannot be invoked to bridge the noted difference in the gravitational potential recovered from analyses of these data by CHASSIS.

This leads us to question the conjecture that phase space samples drawn from independent locations in the galactic phase space should always offer the same unique gravitational potential. The alternative to this is the picture that certain tracer samples will lie confined inside individual potential wells and their kinematic information will therefore betray the details of this local potential well, and not the full galactic potential. In other words, *NGC 3379 is advanced as bistable - perhaps is even multi-stable*. This is the view we now resort to, albeit subject to the remaining assumption that the system is in equilibrium. Also, our inference is true unless the sampling of PNe and/or GC kinematic data are biased in some way. We check for this in Section 9.1.3.

It is to be emphasised that our inference of NGC 3379 being bistable is not synonymous to our recovered test result that the galactic phase space is characterised by regions with distinct phase space density distributions. Instead, a bistable potential structure is a conclusion that is arrived at from the treatment of the relative deviation of the two data samples from isotropy, within CHASSIS.

8.1. Distinct Mass Distributions

Though it is interesting to find that NGC 3379 is multi-stable, we are much more excited to note that the total mass density of NGC 3379 is recovered as distinct, when the two different data sets are used. However, if we view the problem from the context of a Jeans equation formalism, we find that the effect of using two distinct $\sigma_p(r)$ and $\nu(r)$ profiles will in general imply distinct enclosed mass distributions $M(r)$ unless a conspiracy exists between the gradients of these inputs and the modelled anisotropy parameter, to always yield a unique $M(r)$ (discussed in Section 2).

Again, within CHASSIS, we realise that the projection of a trial $f(E)$ into the space of observables (x_p, y_p, v_z), given a trial potential $\Phi(r)$, would yield distinct likelihood structures for distinct input kinematic data - the global maxima in the likelihood function ($\mathcal{L}$) would correspond to distinct $\{\rho - f\}$histogram pairs, i.e. each data set would in general imply distinct mass density distributions as solutions. Here the projection of $f(E)$ into the space of observables is $\mu(x_p, y_p, v_z)$:

$$\mu(x_p, y_p, v_z) = \int f[E(v_x^2 + v_y^2 + v_z^2 + 2\Phi(r))]dv_x dv_y dz \tag{7}$$

and $\mathcal{L} = \ln \sum \mu$. Here the summation is taken over the whole data set.

9. Discussions & Summary

Our results indicate that the mass distribution tracked by the PNe velocities is significantly less than that implied by the GC kinematics! Individual consideration of the PNe analysis leads to a "naked" interpretation for NGC 3379, in line with what was suggested by Douglas et. al (2007) and Romanowsky et. al (2003), though the $\Upsilon(< r)$ recovered from the PNe-RUN, at $5R_E$ (lying between 10 and 20) is slightly higher than what Douglas et. al (2007) advance, due to the assumption of isotropy in our work (which artificially augments $\rho(r)$ - see Section 4.1). The GCs on the other hand imply a dark matter rich system, with $\Upsilon_B(< r) \in$[30, 80], at the 1-σ error level, at about $9R_E$.

Alternative representations of the matter density in NGC 3379 corroborate the same dichotomous picture. These include:

- v_c calculated from the PNe runs concur with the Keplerian fall-off with r but that from the GC runs are significantly flatter (Figure 2).
- the $M(r)$ recovered from the PNe runs flatten by about r=7 kpc. On the other hand, the $M(r)$ recovered from the GC runs is rising even at 25 kpc (edge of the radial extent of the data).

We try to reconcile with the results by asking if we could have misinterpreted something.

9.1. Could We be Wrong?

Is it possible that the assumptions in our analysis have misled us to develop this seemingly dichotomous view of the galaxy? Or could there be a problem related to the collection of the data samples that is causing this view?

9.1.1. Ignoring Anisotropy in Analysis

Would the distinction noted in the $\rho(r)$ recovered with the PNe and GC runs, have vanished if we had not assumed velocity isotropy in our analysis? The answer is no, as explained below.

As discussed earlier in Section 4.1, *the inclusion of anisotropy will render the recovered $\rho(r)$ lower than the profile currently recovered by CHASSIS*. In other words, inclusion of full anisotropy into the analysis of the PNe data will increase the gap between the density profiles recovered from the PNe and GC data. Thus, the only way to reconcile the difference between the density distributions recovered from the PNe runs and GC runs, is to suggest that the GC data are drawn from a phase space distribution that is even more strongly anisotropic than the one from which the PNe data are drawn. However, our statistical testing indicates the exact opposite. This implies that there is no way we can reconcile the differences in the recovered density distributions, by incorporating velocity anisotropy.

9.1.2. Asphericity?

It has been argued that NGC 3379 is actually triaxial rather than spherical (Dekel et. al 2005); the point is that σ_p would then appear deflated for certain inclinations and that this is the reason for the PNS studies to recover spuriously low masses. (Romanowsky et. al 2003; Douglas et. al 2007). Douglas et. al (2007) reject this as improbable, based on the distribution of the intrinsic axial ratios of elliptical galaxies. However, this argument is unacceptable, owing to (i) the obvious errors involved in the constraining of a property of an individual system, knowing only a sample distribution of the characteristic and (ii) the essentially unconstrained nature of the sought distribution of the intrinsic axial ratios.

Within CHASSIS, the *assumption of sphericity involves the geometry of the sought gravitational potential of the system and not that of the tracer spatial distribution.* Also, CHASSIS does not employ the $\sigma_p(r)$ profile derived from observations, but measurements of individual tracer LOS velocities.

If however, the radially symmetric assumption on Φ is misplaced, then this will affect results - the greater the deviation from the assumption of $\Phi = \Phi(r)$, the greater is the expected difference in likelihood structure recovered from using the corresponding data. However, we have indeed checked for the validity of this assumption when we checked for the adherence of an observed data to the assumption of *phase space isotropy*. As explained above, the results of such a test indicate distinct mass density distributions.

9.1.3. GC Data?

It could be argued that the GCs used in our work do not really trace the mass of NGC 3379 but of a shared dark matter distribution that might pervade the inter-galaxy space between NGC 3379 and one or more of its neighbours, among which, NGC 3384 is the closest. But, it is precisely to avoid such a predicament that we use the velocities of only 30 of the GCs that Bergond et. al (2006) advance as definitely belonging to NGC 3379. Besides, interference from the dark halo of a neighbouring galaxy is not expected to explain the significant difference between the recovered $M(r)$ profiles, at 10 kpc. Such effects, if any could kick in at higher radii.

9.1.4. Non-linear Dynamics

It is perhaps likely that a fraction of the PNe and GC orbits are chaotic. Even if this were the case, this does not nullify the observation that the phase space distributions from which the PNe and GC data are drawn are different and that such data imply distinct mass distributions. If anything, the probabilistic measures of the nonparametric $f(E)$ and $\rho(r)$ that CHASSIS provides are the best possible description of the ramifications of non-linearity.

9.2. Risk of using Tracer Kinematics

To sum up the arguments of Section 8.1, we state that in general, kinematic data drawn from distinct phase space densities will yield distinct $M(r)$ profiles and this is not solely because of the issue of phase space isotropy. Thus, for example, within the Jeans equation formalism, it is possible to obtain distinct $M(r)$ using kinematics from two data sets that are drawn from two distinct phase space distributions that are equally anisotropic (as parameterised by the anisotropy parameter $\beta(r)$) - then $d\ln\sigma_p(r)/d\ln r$ and $d\ln\nu(r)/d\ln r$ terms would in general be different in the two cases, even if $\beta(r)$ is the same. In other words, it is not surprising that we think that we have inferred distinct mass density distributions for the same galaxy, using distinct tracer kinematic data.

To put it differently: it is potentially risky to refer to the gravitational potential recovered using an observed tracer sample, as the potential of the galaxy. We have demonstrated this with the example of NGC 3379 and shown that the distinct mass distributions recovered, cannot be made to collapse into consistent forms by invoking the effects of phase space anisotropy, non-linear effects or by attributing errors to the observed GC data.

However, in contrast to PNe and GC samples, if two sets of tracer kinematics can be inferred to have been drawn from the same attractor, we will expect consistency in the gravitational matter density that is recovered by using such data sets in a mass determination formalism. Such a possibility is discussed in the following section.

9.3. Distinct Phase Space Distributions & Multi-stability of NGC 3379

We have seen that in Section 4.3 that the *phase space of the galaxy NGC 3379 is actually marked by distinct basins of attractions*, otherwise we cannot explain the noted difference in the recovered solutions for mass density, given that two independent data samples drawn from distinct distribution functions. We use the differential adherence of the two data to isotropy, to conclude that the system is bistable and is perhaps multi-stable. Such a result should not really surprise us, given that, at least on local scales, the phase space structure of the Galaxy is highly multi-modal and the ensuing dynamics is highly non-linear, marked by significant chaoticity (Chakrabarty & Sideris 2008; Chakrabarty 2007; Quillen 2003).

After all, even a potential structure as simple as $Ar^2 + Br^4$ is bistable (A and B being scalar constants); thus, model galactic potentials which are typically represented as superposition of analytical potentials of individual galactic components can indeed manifest multi-stability. That galactic potentials are multi-stable and deviate - over varying length scales - from smooth analytical forms is perhaps more in line with the idea that galaxies, viewed as dynamical systems, are expected to manifest complexity.

Beyond the mere identification of such multi-stability, the much more involved issues are - what causes this multi-stability and what are the physical processes/time scales involved in the escape of an orbit from the well it is trapped within and migrate from one one basin of attraction to another. It is possible that *such a configuration arises from the modification of the system, introduced by the action of resonant perturbations or dissipation* (Chizhevsky, Corbalan & Pisarchik 1997; Mendes 2000)[4]. .

9.3.1. Possible causes of phase space splitting

We consider the dynamics of the tracer populations to be dissipationless and our treatment of the galaxy as a dynamical system rules out dissipation due to interaction with external systems. We undertake this simplified idealised picture even while appreciating that the details in a system as messy as a galaxy are perhaps less idealised and internal sources of dissipation exist.

However, resonant perturbations from interaction of the different components of the galaxy are possible, eg. interaction with the outer tumbling halo, as discussed by Dubinski & Chakrabarty (2009). Primarily, distinct phase space density distributions can be triggered by the different evolutionary histories of PNe and GCs. PNe are basically the end states of (low to medium mass) stars. Thus, it is envisaged that the phase space density that describes PNe motion will be similar to that of old, low to medium mass stars. In that case, PNe velocity data and the kinematics of such a stellar population will be drawn from the same part of the galactic phase space and the recovered $M(r)$ will be consistent in these two cases.

9.3.2. Escaping confining potential well

A detailed study of the structure of phase space is required to answer questions about the efficacy of a certain fraction of phase space to lead to an attractor and the time-scales of confinement of orbital samples in a given basin of attraction. Such a study calls for the identification of damping, once the bistable potential structure is established. Studying this in the light of the physics of galactic evolution is an interesting exercise, to be considered for the future.

[4] It is shown that such weak periodic perturbations induce two or more attractors in the system in place of the one initial attractor, rendering the system *bistable* (Ott 1993; Banerjee 2003). A small amount of introduced dissipation can also cause conservative systems to develop multiple attractors. Such is possible in NGC 3379. The original primary attractor is split into multiple new attractors, one of which could be that subset of the galactic phase space that can describe the GC orbital distribution while the other could explain the PNe orbits

9.4. "Naked Galaxies"

The upshot is that the splitting of the entire orbital distribution into two or more distinct basins of attractions, is not improbable. When such occurs, it is possible to fall prey to our ignorance about the galactic phase space structure, and infer spurious galactic properties based on the characteristics of one of these distinct regions of phase space. Expectedly, increasing the range of measurements to multiple tracer classes, will only help to impose tighter constraints on the solution.

It is possible, that the low DM content of the 5 "naked" galaxies, (Romanowsky et. al 2003) was achieved as a result of this situation. Incorrect mass distributions can emanate from substituting information about the galactic phase space by that of orbital distribution of an observed tracer sample that might be drawn from one of the wells in the multi-stable potential structure. Scanning over a wide range of the parameterisation of velocity anisotropy, is not enough in general, to compensate for the errors caused by this substitution. Thus, cross-validation of results obtained with different tracer classes, wherever possible, is welcome.

9.5. True Mass Distribution

At the end of the discussion presented above, we will naturally want to know what the true mass distribution of NGC 3379 is. However, in light of the knowledge that the system potential is multi-stable, unless we are sure that the kinematic sample at hand does not correspond to orbits that are confined to a local potential well, we cannot answer the question of what the true galactic potential is, on the basis of any analysis of such a sample. All we can characterise is the local potential well that the sample is drawn from. However, the gravitational potential of the galaxy is a superposition of the individual wells and hence we can at least put a lower bound on the total gravitational mass content of the galaxy, using analyses of tracer kinematics. This is presented below.

Thus, NGC 3379 is advanced as a dark matter rich galaxy, with $\Upsilon_B(< r)$ at least as high as to lie in [30, 80], at a radius just inner to 20 kpc ($r \approx 9R_{eff}$). The enclosed mass at this radius is at least as high as about 4 to $10\times10^{11}\mathrm{M}_{\odot}$. Enhancement of the GC data sample will reduce these errors of analysis.

We conclude that it is risky to refer to the mass distribution recovered upon application of tracer kinematics, as the mass distribution of the galaxy.

10. Conclusions

In this work we advance the idea that the galaxy NGC 3379 is at least bistable, (if not multi-stable) on the basis of the fact that a robust Bayesian non-parametric analysis of the kinematic information of two distinct tracer samples, leads to significantly different (at 1-σ level of significance) gravitational mass density distributions. This difference in the mass density is shown to not diminish on the imposition of appropriate amounts of correction - in terms of inclusion of anisotropy - on the analysis of the two data sets. Thus, we are led to believe that the data characterise tracer orbits that live in distinct potential wells in the galaxy, i.e. the galaxy is bistable.

Galaxies are such messy and complex systems that it is only to be expected that they should be multi-stable. In fact, what would be surprising is anything otherwise. The possibility of multi-stability is not moot, rather what is challenging is the estimation of probabilities of orbital escape from individual potential wells and efficiencies of migration across the landscape of the galactic phase space, as computed within the paradigm of galactic evolution.

Acknowledgements. I am indebted to Aaron Romanowsky for his kind supplying of the data. It is a pleasure to acknowledge the very insightful comments and suggestions of Carlos Pereira and Paulo Cilas Marques Filho, towards the strengthening the Bayesian significance testing, undertaken here. I also acknowledge the help of Michael Allman for his comments. The author was supported by

a Royal Society Dorothy Hodgkin Research Fellowship in the beginning of this work and later supported by the Warwick Centre of Analytical Sciences Fellowship.

References

Banerjee, P., 2003, *Nonlinear Optics Theory, Numerical Modeling and Applications*, Marcel Dekker Inc., New York, Basel.

Basu, D., 1975, *Sankhya A*, 37, 1.

Bergond, G., Zepf, S. E., Romanowsky, A. J., Sharples, R. M., & Rhode, K. L., 2006, A&A, 448, 155.

Birnbaum, A., 1962, *Jl. of the American Statistical Association*, 57, 269.

Chakrabarty, D., 2009, *accepted for publication in Astronomy & Astrophysics*.

Chakrabarty, D., 2009, *Proceedings of the 18th IMACS World Congress MODSIM 2009, Cairns*, arXiv:0905.2524.

Chakrabarty, D., Raychowdhury, S., 2008, AJ, 135, 2350.

Chakrabarty, D., and Sideris, I. V., 2008, A&A, 488, 161

Chakrabarty, D., 2007, A&A, 467, 145.

Chakrabarty, D., 2006, ApJ, 131, 2561.

Chakrabarty, D., and Portegies Zwart, S., 2004, ApJ, 128, 1046.

Chakrabarty, D., and Saha, P., 2001, ApJ, 122, 232.

Chizhevsky, V. N., Corbalan R., & Pisarchik, A. N., 1997, *Physical Review E*, 56, 1580.

Côté, P., McLaughlin, D. E., Cohen, J. G., & Blakeslee, J. P., 2003, ApJ, 591, 850.

Côté, P., McLaughlin, D. E., Hanes, D. A., Bridges, T. J., Geisler, D., Merritt, D., Hesser, J. E., Harris, G. L. H., Lee, M. G., 2001, ApJ, 559, 828.

de Lorenzi, F., et al., 2009, MNRAS, 395, 76.

Dekel, A., Stoehr, F., Mamon, G. A., Cox, T. J., Novak, G. S., & Primack, J. R., 2005, Nature, 437, 707.

Douglas, N. G., et a., 2007, ApJ, 664, 257.

Douglas, N. G., et. al, 2002, PASP, 114, 1234.

Dubinski, J., and Chakrabarty, D., 2009, ApJ, 703, 2068.

Gelman, A., Carlin, J., Stern, H., & Rubin, D., 1995, *Bayesian Data Analysis*, Chapman and Hall.

Gelman, A., Roberts, G., O. & Gilks, W., R., 1996, *Bayesian Statistics 5*, ed. J. Bernardo et al., Oxford University Press, 599.

Hastings, W. K., 1970, *Biometrika*, 57, 97.

Hubbard, R. & Lindsay, M. R., 2008, *Theory and Psychology*, 18, 69.

Kempthorne, O. & Folks, L., 1971, *Probability, Statistics and Data Analysis*, Ames, I0: Univ. of Iowa Press.

Koopmans, L. V. E., 2006, EAS Publications Series, 20, 161.

Łokas, E. L., & Mamon, G. A., 2003, MNRAS, 343, 401.

Madruga, R. M., Luis E. G. & Wechsler, S., 2001, *Test*, 10, 291.

Mendes, V., *Dynamical systems: from crystal to chaos*, 2000, eds. J. M. Gambaudo, P. Hubert, P. Tisseur, S. Vaienti, World Scientific, 105.

Metropolis, N., Rosenbluth, A. W., Rosenbluth, M. N., Teller, A., & Teller, H., 1953, *Jl. of Chemical Physics*, 21, 1087.

Ott, E., 1993, *Chaos in Dynamical Systems*, Cambridge University Press, Cambridge, UK.

Pellegrini, S., and Ciotti, L. 2006, MNRAS, 370, 1797.

Pereira, C. A. de B., Stern, J. M. and Wechsler, S., 2008, *Bayesian Analysis*, 3, 79.

Pereira, C. A. and Stern, J. M., 1999, *Entropy*, 1, 99.

Quillen, A. C., 2003, AJ, 125, 785.

Roberts, G., Gelman, A. and Gilks, W., 1997, *The Annals of Applied Probability*, 7, 110.

Roberts, G. and Sahu, S., 1997, *Journal of the Royal Statistical Society. Series B*, 59, 291.

Roberts, G. and Rosenthal, J., 2001, *Statistical Science*, 16, 351.

Romanowsky, A. J. et al., 2003, *Science*, 301, 1696.

Sambhus, N., Gerhard, O., & Méndez, R. H., 2006, AJ, 131, 837.

Sambhus, N., Gerhard, O., & Méndez, R. H., 2005, *Planetary Nebulae as Astronomical Tools*, 804, 317.

Sawyer Hogg, H., 1947, *Journal of the Royal Astronomical Society of Canada*, 41, 265.

Tanner, M. A., 1996, *Tools for statistical inference*, Springer-Verlag, New York.

Thompson, J. M., and Stewart, H. B., 2001, *Non-linear dynamics and chaos*, Wiley.

Tierney, L., 1994, *The Annals of Statistics*, 22, 1701.

Weijmans, A. M., et al., 2009, MNRAS, 398, 561.